13th ewtec 2019 Proceedings of the 13th European Wave and Tidal Energy Conference 1-6 Sept 2019, Naples, Italy

The Effects of Inflow Turbulence Intensity on predicting wake velocity in a two dimensional RANS Actuator disc model

Chee M. Pang, David M. Kennedy, and Fergal O'Rourke

Abstract— **The RANS Actuator disc model has been commonly and widely used in the both wind and tidal energy to predict the wake of a horizontal axis turbine. This method has the advantage of giving accurate results at an affordable computing cost. A 2 dimensional actuator disc technique is a simple method which produce a similar far wake in comparison to the real turbine. The use of this method reduces the mesh density required and reduces some of the scaling issues faced by other methods of analysis. The model is a good choice especially when considering array layouts or environmental impacts, i.e. where large-scale effects of the turbine on flow are of interest. The accuracy of the model for evaluating the wake of the tidal stream turbine is affected by multiple variables, such as the turbulence model, turbulence intensity, porosity, loss model, etc. This paper discusses the effect of varying the inflow turbulence intensity on solving the RANS-Actuator disc in k–ω SST (shear stress transport) turbulence model in CFD simulations. Particular attention is given to the rate of wake recovery, turbulence intensity and velocity deficit. The work is also validated against experimental measurements and existing 3-dimensional RANS-Actuator disc models found in the literature. The validation shows the model is accurate and can be used to predict turbine performance at different intensities. It can therefore be applied to predict performance of turbine with operating in real tidal site conditions.**

Keywords—**CFD, tidal turbine, wake, tidal energy, actuator disc, RANS**

I. Introduction

MARINE currents possess some advantageous characteristics over other renewable resources such as high predictability and availability. Tidal cycles are very predictable with time-varying flow and direction, which is ideal for optimised energy output [1],[2]. The concept of extracting kinetic energy from marine currents is a fairly old idea and in more recent years, this energy source has seen successful full-scale prototype development and testing with a number of commercial-scale devices with various companies around the globe working on different forms of tidal stream turbines (TST). The marine energy resources are mostly concentrated at comparatively compact sites where the flows are spatially constrained such as around estuarine inlets, headlands or between islands [3]. According to the Betz limit, for TST technology, to achieve optimum electricity production on a commercial-scale, turbines will have to be installed in arrays or farms to maximise the extractable power [4],[5]. To determine the optimal turbine array layout, several investigations have been undertaken to study the effects of array scale and configuration on the power output. Furthermore, energy extraction by TSTs induces a wake flow which may disturb the downstream tidal current flow and the performance of the downstream TSTs [6]. Thus, it is crucial to study turbine wake development.

There are a number of approaches that can be utilised to model the wake effects of a tidal current turbines. However, the actuator disc approach has been widely used to represent the turbine employing the Reynolds-Averaged Navier-Stokes (RANS) equations. This approach estimates the force exerted on the flow field by the turbine, which is represented by a porous disc. The benefit of solving the RANS equations using actuator disc model is the significant improvement in the computational efficiency of the Computational Fluid Dynamics (CFD) simulation, since the model does not required an elaborately detailed mesh, to capture for example boundary layer conditions, and can be solved in a steady-state solution [7]. Although this method has significant computation benefits in modelling a tidal stream turbine, the assumptions made in this approach can cause inaccuracies in the physical representation of near wake of a turbine.

There are three fundamental assumptions made for the purpose of this work. Firstly, the disc is non-rotating therefore eliminating any swirl in the flow. Beyond the near wake, which is generally beyond 5D downstream, has a similar structure of that of a turbine [8]. Swirl in the

No. 1758, Tidal Hydrodynamics Modelling

C. M. Pang is with the Centre for Energy and Renewables at Dundalk Institute of Technology, Dundalk, County Louth, Ireland (e-mail: CheeMeng.Pang@dkit.ie)

F. O'Rourke is with the Centre for Energy and Renewables at Dundalk Institute of Technology, Dundalk, County Louth, Ireland (e-mail: fergal.orourke@dkit.ie)

D. M. Kennedy is with the Department of Mechanical Engineering, Dublin Institute of Technology, Bolton Street, Dublin 1, Ireland. (e-mail: david.kennedy@dit.ie)

near wake can persist further downstream potentially influencing the flow boundaries and cause distortion in the wake [9]. Secondly, it is assumed that tip vortices from rotating turbine blade were ignored due to the actuator disc's inability to replicate these vortices [10]. Thirdly, transient flow characteristics are not account for in the steady-state actuator disc-RANS model. This model provides information about mean flow and assumed isotropic turbulence. Hence, it is useful in understanding the characterises of the flow behind the turbine [11]. Numerous studies have been carried out on tidal stream turbines using the actuator disc-RANS model and the predictions of the velocities in the wake and velocities recovery varied significantly [11]. According to studies done by Harrison M.E., et al. (2010) from University Southampton [7] and V.T. Nguyen from Hanoi University [12], the rate of recovery is dependent on the inlet turbulence intensity and turbine-induced turbulence, this would greatly affect the near wake velocities but the far wake has comparable similar wake velocities in both cases.

A significant number of investigations have been undertaken primarily on the performance of individual devices operating at optimum conditions. However, from the published literature on offshore wind farms, it is observed that offshore wind farm arrays with multiple rows will encounter wake-shadowing effects. Therefore, this suggest that other than the first row, units of subsequent rows will operate in weaker incoming flow conditions comparing to the first row[13]. Hence, it is important to investigate the effect of non-ideal incoming flow on the turbine, in particular the effects of turbulence intensity.

In this work, a computational investigation is conducted on the effects of different inflow turbulence intensities on predicting the decay of velocity deficit and turbulence in the downstream wake of the tidal turbine. The CFD model is validated by comparisons with existing experimental and numerical measurements found in the literature [7] ,[12].

II. THEORY

A. Reynolds-Averaged Navier–Stokes (RANS) equations

The approximated forces exerted on the flow by the turbine are applied as source terms in the RANS equations of momentum conservation given in (1) [14] ,[15], and are solved along with the continuity equation seen in (2) [14] ,[15].

$$\frac{\partial(\rho U_i)}{\partial \mathrm{t}} + \frac{\partial\left(\rho U_i U_j\right)}{\partial x_j} = -\frac{\partial \mathrm{P}}{\partial x_i} + \frac{\partial}{\partial x_j}\left[(\mu + \mu_t)\left(\frac{\partial U_i}{\partial x_j} + \frac{\partial U_j}{\partial x_i}\right)\right] + \rho g_i + S_i \quad (1)$$

$$\frac{\partial U_i}{\partial x_i} = 0 \quad (2)$$

The source terms are only applied at elements within the turbine region and the Euler notation is used in these equations for brevity given in (2) [14]. Where ρ is the density of water, U_i is the velocity of the water averaged over time, t, x_i is the spatial distance, μ is the dynamic viscosity of water, μ_t is the eddy viscosity, g_i is the component of gravitational acceleration and S_i is an added source term.

B. Momentum loss in CFD simulations

The actuator disc applies a resistance to the incoming flow. This resistance causes the actuator disc to experience force similar to that of a turbine operating under the same conditions. Therefore, the standard Reynolds-averaged momentum equation, given in (1), applies to the fluid region and the porous region and is defined with an isotropic loss model based on a generalised form of the Darcy-Weisbach equation as seen in (3) [14]:

$$S = -\left(\frac{\mu}{K_{perm}} U + K_{loss}\frac{\rho}{2} U^2\right) \quad (3)$$

where K_{perm} is the porous region permeability and K_{loss} is loss coefficient. The permeability of the porous region, K_{perm}, can be determined using Darcy's Law as seen in (4) [16]. While the loss coefficient of the porous region, K_{loss}, is defined as the gradient across the disc thickness given in (5) [14].

$$K_{perm} = \frac{Q\mu L}{A\Delta P} \quad (4)$$

$$K_{loss} = \frac{k}{L} \quad (5)$$

where Q is the volumetric flow rate through a permeable medium, L is the length over which the pressure change takes place, A is the turbine area, ΔP is the pressure change across the porous region and k is the resistance coefficient of the porous region.

C. Actuator Disc theory

In the actuator disc theory, a thrust force, F_T is homogeneously distributed across the disc which represents the tidal current turbine. However, the disc cannot replicate swirl caused by the rotating turbine rotor in the near wake between 2D to 5D. However, there is no difficulty solving the far wake flow field. The thrust force acting on the disc results in a discontinuity in pressure, a reduction of kinetic energy of the flow and a decrease in flow velocity downstream. The thrust force, F_T is

calculated with (6) [17] where C_T is the thrust coefficient and U_∞ is the upstream flow velocity.

$$F_T = \frac{1}{2} C_T \rho A {U_\infty}^2 \quad (6)$$

According to the Betz limit, the maximum ideal power from the tidal current flow occurs when axial induction factor, a, is at 0.33 which results in a power coefficient and thrust coefficient of 0.59 and 0.88 respectively. The relationship between thrust coefficient and axial induction factor is clearly demonstrated in (7) [18] and the relationship between power coefficient and axial induction factor is given in (8) [18].

$$C_T = 4a(1-a) \quad (7)$$

$$C_p = 4a(1-a)^2 \quad (8)$$

According to Taylor [19], a relationship can be formed between open area ratio or porosity, θ, and the resistance coefficient, k, as shown in (9). This relationship has been examined by Whelan [20] which shows this relationship as a reasonable approximation. The resistance coefficient, k, can also be determined using axial induction factor, a, given in (10).

$$\theta^2 = \frac{1}{1+k} \quad (9)$$

$$k = \frac{4a}{1-a} \quad (10)$$

III. METHODOLOGIES

D. Numerical Method

The transport equations were solved using ANSYS CFX which solves the Navier-Stokes mass and momentum equations [14]. CFX uses a hybrid of finite volume and finite discretisation methods, allowing CFX to solve any mesh topography. A previous similar study presented by Harrison et. al. indicates that the utilisation of k-ε turbulence model within the RANS simulation does not accurately model the flow condition [7] and the k–ω SST (shear stress transport) turbulence model under-predict the eddy-viscosity and hence under-predict the rate of wake recovery [11]. The k–ω SST model is popular in solving turbulence closure for external flows particularly airfoil type problems. The k–ω SST model is a hybrid of k–ω and k-ε expressed in k–ω form with shear stress limiting near solid boundaries. However, the actuator disc model has no solid boundaries associated with blades, hence the model would revert back to the k-ε model [21]. Therefore, for these conditions, the k–ω SST model seems to behave similarly to the k-ε model but k–ω SST model, according to Johnson, performs better in flows featuring pressure gradients in terms of accuracy to predict flow properties [22].

It was concluded that an improved agreement was reached by introducing turbulence sources at the disc to represent he turbulence produced. In this work, the model is assumed to be time invariant and the flow field problem was solved in a two-dimensional domain with the top, bottom and outlet of the domain treated as opening entrainment boundary conditions with zero gradient instead of walls to eliminate the effects of wall shear on the wake results.

E. Domain Dimensions and Conditions

The 2-dimensional fluid domain has a dimension of 30D by 30D with a thickness of 1mm. The disc is located mid-depth about 15D from the top wall and 5D away from the domain inlet. The disc is 1m in diameter and 0.1m in thickness. The fluid domain was modelled with the SST model and the actuator-disc domain was described as a porous domain with the volume porosity determined using Equation (9) and was calculated based on betz limit of C_p value 0.59. The loss model of the porous domain was modelled as true velocity isotropic loss with permeability and resistance loss coefficient determined using Equations (4) and (5). The actuator-disc domain parameters are summarised in Table I.

TABLE I
POROUS DISC DOMAIN PARAMETERS

Parameters	Value
Volume Porosity, θ	0.58
Loss Model Type	Isotropic Loss
Resistance Coefficient, K	2.0
Resistance Loss Coefficient, K_{loss}	20 m^{-1}
Permeability, K_{perm}	2.51 x10^{-7} m^2

F. Boundary Conditions

The top, bottom and outlet faces were described as opening boundaries with entrainment conditions with zero relative pressure and zero turbulence gradient. The velocity at the inlet boundary was defined as a normal inlet velocity of 0.8m/s with the k-ε turbulence model. The turbulence at the inlet boundary was defined in terms of the turbulent kinetic energy, k, and eddy dissipation, ε, which were calculated from Equations 11 and 12 respectively, for varying turbulence intensity.

$$k = \frac{3}{2} I^2 {U_\infty}^2 \quad (11)$$

$$\varepsilon = \frac{k^{3/2}}{0.3 D_h} \quad (12)$$

where I is the turbulence intensity and D_h is the depth of the water. Fig. 1 shows the inlet velocity and

turbulence intensity 2D from the inlet at turbulence intensity of 5% and the measured data by Harrison [7]. It is seen that the model inlet velocity provided a reasonable match with measured data, but the turbulence intensities did not match closely with the measured data.

TABLE II
BOUNDARY CONDITION PARAMETER

Parameter (Face)	Setting
Inlet	Normal inlet speed, k-ε turbulence model base on (11) and (12)
Top and Bottom	Opening, Entrainment, 0 Pa
Outlet	Opening, Entrainment, 0 Pa
Left and Right	Symmetry

Further investigations are required to explore these discrepancies. The parameter setting of each boundary is summarised in Table II.

G. Mesh Convergence Studies

A mesh convergence study was conducted by increasing the number of elements within the computational fluid domains. However, this was achieved by only increasing the mesh density around the most significant regions of the flow field and leaving the global mesh area unchanged as shown in Fig. 2.

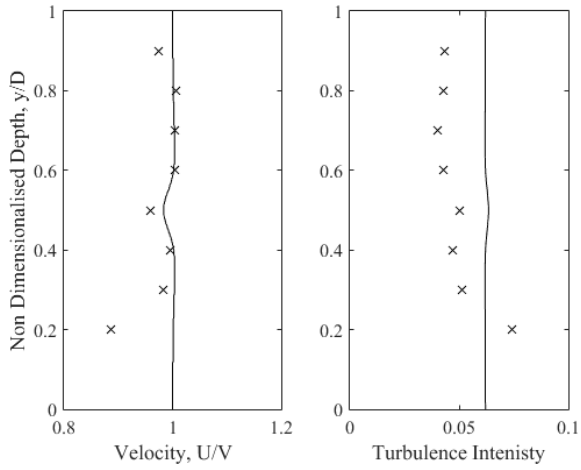

Fig. 1. Vertical velocity profile and turbulence intensity at 2D from the inlet comparing with measured data [7].

This method significantly reduces the computational requirements needed to solve the simulation by prioritising the area with high velocity gradients. The basic structured mesh has around 3.12 $x10^4$ number of elements and 6.39 $x10^4$ number of nodes which is suitable for the SST turbulence model. Four different computational meshes with increasing number of elements and nodes were constructed to investigate the effect of mesh density on centreline velocity, C_P and C_T for the actuator disc as shown in Table 4. Fig 3. shows the velocity profile 7D downstream, in the figure the wake profile velocity decreases slightly as mesh density increases. However, at mesh density above 4.64 $x10^5$ number of elements and 9.93 $x10^5$ number of nodes, the profiles show little changes.

TABLE III
COMPUTATIONAL DEVICES SPECIFICATION

Device Hardware	Specification
Processor	Intel Core i7-7700HQ CPU 2.80GHz
RAM	8.00 GB
System type	64-bit Microsoft Operating System
Storage Type	100GB Solid State Drive
Processor	Intel Core i7-7700HQ CPU 2.80GHz

The mesh converged at proximately above 4.64 $x10^5$ number of elements and 9.93 $x10^5$ number of nodes as shown in Table 4, the downstream velocity ceased to change after 4.64 $x10^5$ number of elements. Both the C_P and C_T value converge at 4.64 $x10^5$ number of elements with values of 0.376 and 0.645 respectively. The computation time required by the solver to solve at this mesh density is approximately 1 hours 4 minutes and 3 seconds under the computational specification mention in Table III.

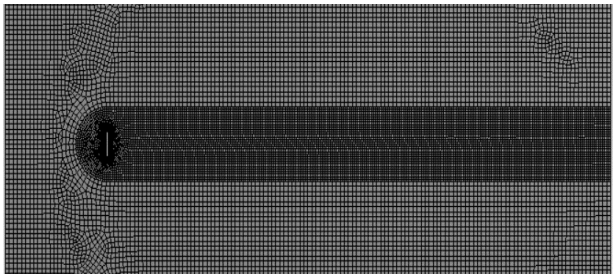

Fig. 2. Computational mesh showing high density mesh in the actuator disc region and the wake downstream of the actuator disc.

IV. RESULTS AND DISCUSSION

H. RANS-Disc Model Validation

A validation study was conducted on the constructed RANS actuator-disc model, the model was validated against the experimental data by Harrison and the numerical models by Harrison and Nguyen. The velocity downstream from the mid-centreline of the actuator disc

TABLE IV
EFFECTS OF INCREASING NUMBER OF ELEMENTS AND NODES ON C_T, C_P AND CENTRELINE AT 5D, 7D AND 10D

No. of elements	No. of nodes	C_T	C_P	Centreline Velocity at Downstream (m/s)			total time
				5D	7D	10D	(hour: minute: second)
$3.11x10^4$	$6.39x10^4$	0.649	0.379	0.473	0.535	0.594	00:15:10
$1.17x10^5$	$2.37x10^5$	0.648	0.378	0.473	0.536	0.595	00:23:37
$4.64x10^5$	$9.33x10^5$	0.645	0.376	0.474	0.537	0.596	01:04:03
$1.13x10^6$	$2.27x10^6$	0.646	0.377	0.474	0.537	0.596	03:28:06

of the model was validated against the mentioned experimental and numerical model as shown in Fig. 4. The RMSE value of Harrison and Nguyen models to the current work were 0.0375 and 0.0553 respectively, while the RMSE value of the current work to the experimental data is 0.0370. The values of root mean square error (RMSE) indicate excellent correlation with previous studies in this domain.

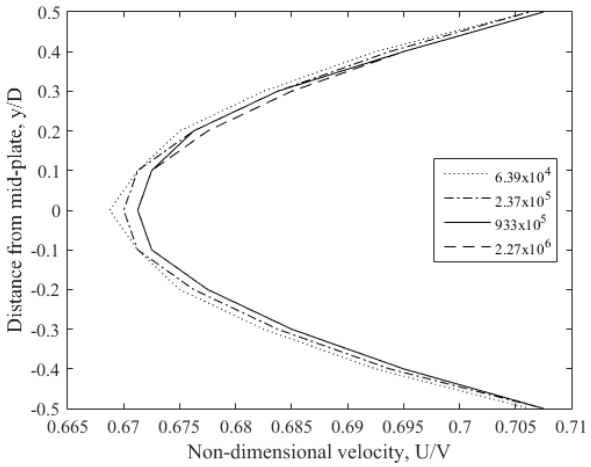

Fig. 3. Vertical wake velocity profile at 7D downstream of the disc. Comparison between different mesh densities.

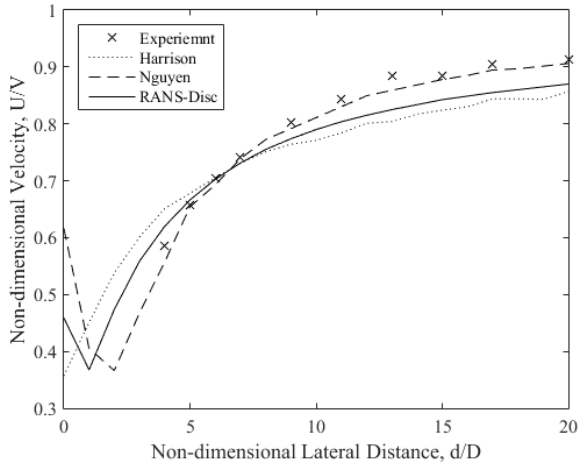

Fig. 4. Non-dimensional velocity along the centreline of the actuator disc downstream of the actuator disc. Comparison between experimental [7] and numerical results[12].

Fig. 5 and 6 show the comparison of velocity and turbulence intensity between the RANS-Disc model at 5% inlet turbulence intensity and Harrison's experimental data at 4D, 7D, 11D, 15D and 20D downstream of the actuator disc. The velocity profile at 5% inlet turbulence intensity closely matches the experimental data particularly the near wake velocity profile as seen in Fig. 5. However, the turbulence intensity of the model at 5% compares well with experimental data, as seen in Fig. 6. The use of the k−ω SST (shear stress transport) turbulence model, as mentioned in the methodology section, are similar to the numerical approach taken by Harrison. In this model the vertical velocity profile matched closely with the experimental data. However, this work concluded that the SST turbulence model under-predicts the rate of wake recovery in turbulence intensity, this may be due to the changes made in the inflow turbulence intensity. Further details of vertical velocity and turbulence intensity profiles for inlet turbulence intensity of 3% and 7% are given Appendix 1.

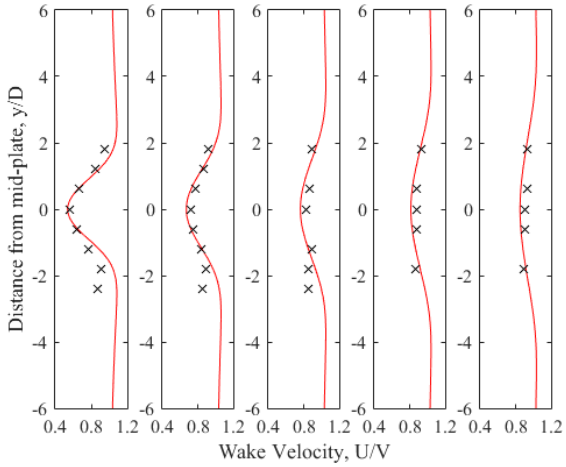

Fig. 5. Vertical profiles of axial normalised velocity at 4D, 7D, 11D, 15D and 20D (shown from left to right) downstream of the disc. Comparison between numerical investigation and experimental results [7].

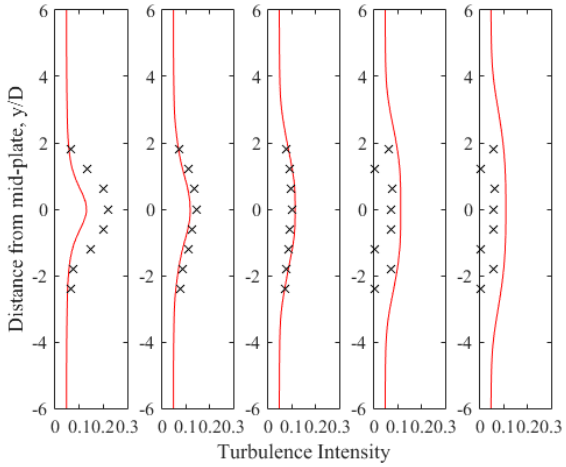

Fig. 6. Turbulence intensity profile at 4D, 7D, 11D, 15D and 20D (shown from left to right) downstream of the disc. Comparison between numerical investigation and experimental results [7].

I. Wake Velocity Study

The wake velocity downstream behind the actuator disc recovers as it moves further downstream from the actuator disc. It is observed that the velocity deficit is significant in the near wake (i.e. less than 5D) with a deficit of more than 40% at the mid-depth of the actuator disc, as shown in Fig. 7. Whereas, the wake shows significant recovery after 10D with a deficit of less than 25%. Wake deficit is the highest at the mid-depth position of the actuator disc regardless of lateral distance. Refer to

Appendix 2 for the wake velocity deficit at inlet turbulence intensities of 3%, 7%, 10% and 15%.

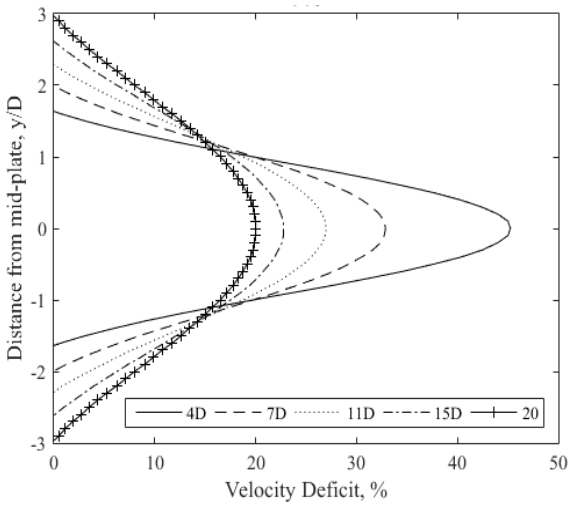

Fig. 7. Vertical wake velocity deficit profile at lateral distance of 4D, 7D, 11D, 15D and 20D at the inlet turbulence intensity of 5%.

As the inlet turbulence intensity increases, the rate of wake recovery increases also. Fig. 8 shows that at a lower inlet turbulence intensity of 3%, the near wake experiences a decrease in velocity and slowly recovers moving into the far wake of the actuator disc as seen further in velocity contour in Fig. 9. Whereas at an inlet turbulence intensity of 7%, and above, the decrease in velocity is less significant with greater recovery in the far wake as shown in velocity contour in Fig. 9. The same occurs for the power available in the wake downstream of the actuator disc, i.e. as the inlet turbulence intensity increases, the power in the wake increases and recovery occurs faster as shown in Fig. 11. Whereas, the increase in inlet turbulence intensity increases the fluid flow's overall turbulence intensity. The turbulence intensity recovers to a new steady value with each increasing inlet turbulence intensity as shown in the turbulence intensity contour in Fig.10. In Fig. 10 it is observed that the global intensity increases as the inlet intensity increases.

Although the increase in inlet turbulence intensity increases the rate of wake recovery, the power coefficient, C_P, on the actuator disc decreases as the inlet turbulence intensity increases as shown in Fig. 12. Using a low inlet turbulence intensity model (3%), the actuator disc will have a higher C_P but the near wake recovers slower and the downstream velocities experience a considerable drop. Conversely, for high inlet turbulence intensity models (above 7%), the actuator disc experiences a decrease in C_P but the wake recovers faster and the downstream velocity experiences little deficit. Hence, the middle range inlet turbulence intensity model (5% to 7%) is the ideal intensity selection with the optimum configuration for both power on the actuator disc and wake recovery. The 5% inlet turbulence intensity was used to validate with existing model and was able to predict results closes to those models.

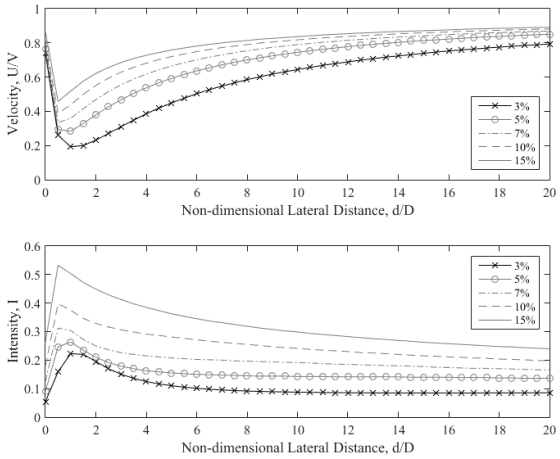

Fig. 8. Non-dimensional velocity and turbulence intensity along the centreline of the actuator disc downstream of the actuator disc at inlet turbulence intensities of 3%, 5%, 7%, 10% and 15%.

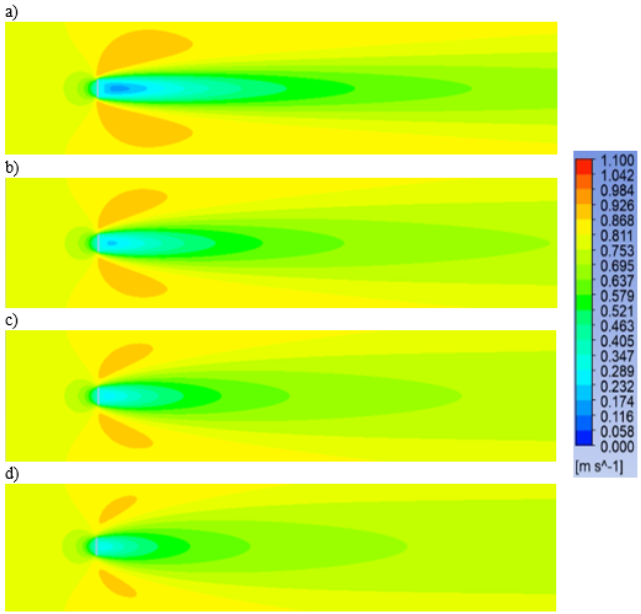

Fig. 9. ANSYS CFX RANS-Disc model velocity contour at inlet turbulence intensities of a) 3%, b) 5%, c) 7% and d) 10%.

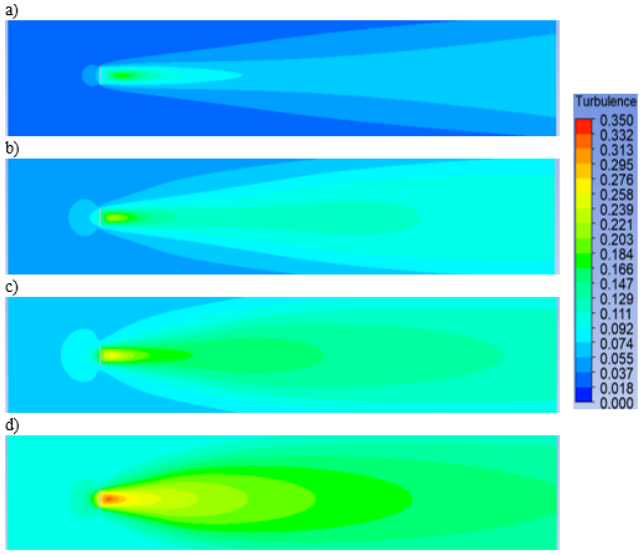

Fig. 10. ANSYS CFX RANS-Disc model turbulence intensity contour at inlet turbulence intensities of a) 3%, b) 5%, c) 7% and d) 10%.

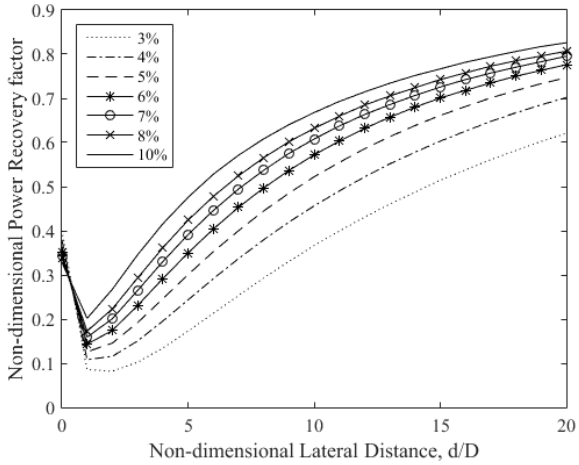

Fig. 11. Non-dimensional power recovery factor downstream of the actuator disc at the mid-centreline position.

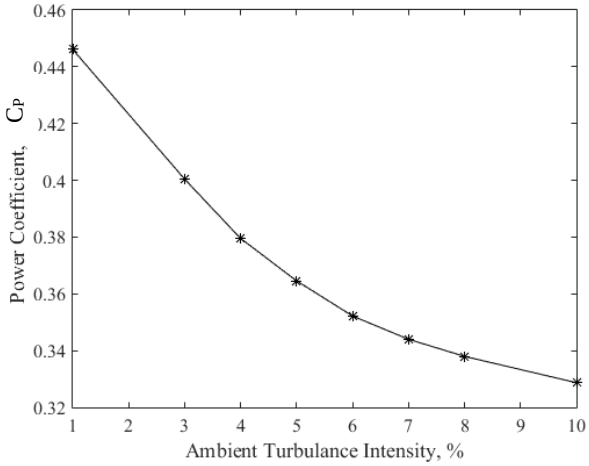

Fig. 12. Power coefficient of the actuator disc at a range of inflow turbulence intensities.

V. Conclusion

This work presents a model to evaluate the effects of turbulence intensity on power and velocity recovery in the wake of a tidal current turbine using an actuator disc approach. The model was setup using Ansys CFX. From comparing with other existing models, this work has demonstrated high accuracy in modelling the wake profile of a tidal current turbine. However, the use of the SST turbulence transport model solve the wake profile under-predicted the near wake profile. From the studies in the literature, it was observed that when the ambient turbulence intensity increases, the power on the actuator disc decreases. The ideal turbulence intensity has proved to be in the mid-range turbulence intensity of between 4% to 7%. The actuator disc model, regardless of intensity, reduces to less than 20% in velocity deficit for downstream distances of 10D to 12D, suggesting that a second turbine could be placed at this position in a tidal current turbine array arrangement.

The further work on this important area include studies such as investigating the effects of different inlet turbulence models has in predicting the wake of a turbine, the effects of siting multiple turbines on the flow field, the effect of yaw misalignment and also predicting the array layout and power output of a real tidal energy site.

VI. Appendix

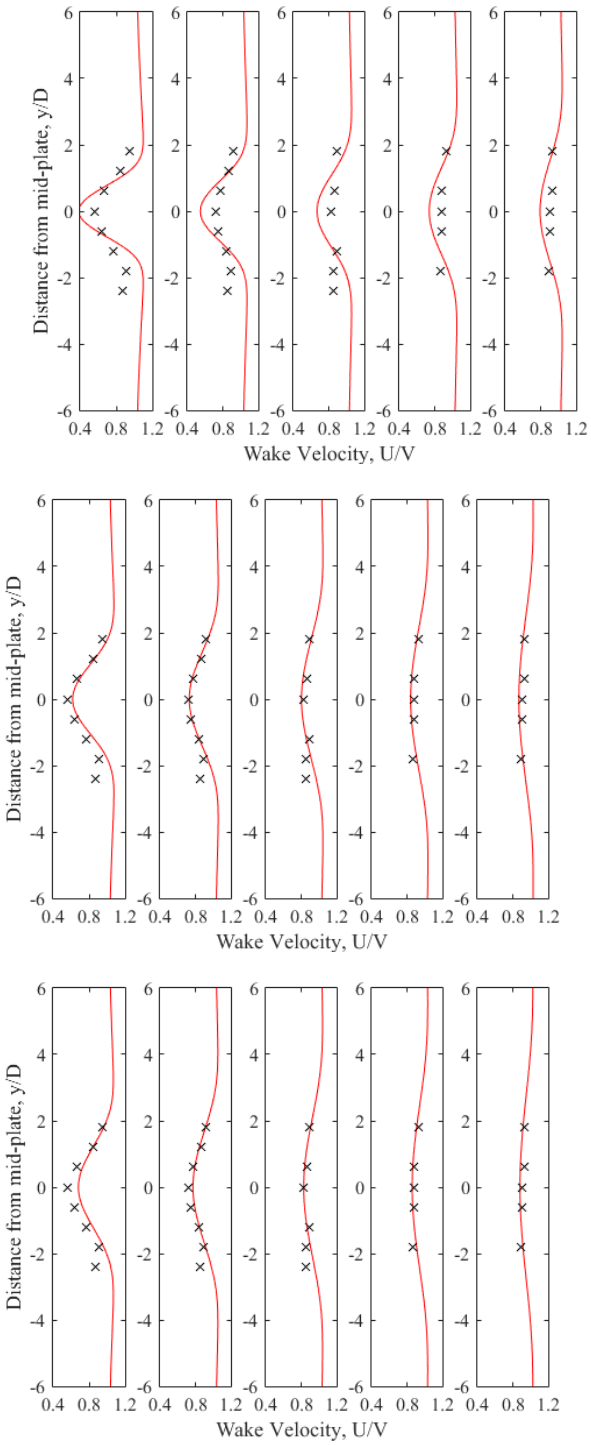

(a) Wake velocity at inlet turbulence intensity of 3% (Top) at 4D, 7D, 11D, 15D and 20D (shown from left to right), 7% (middle) at 4D, 7D, 11D, 15D and 20D (shown from left to right) and 10% (bottom) at 4D, 7D, 11D, 15D and 20D (shown from left to right).

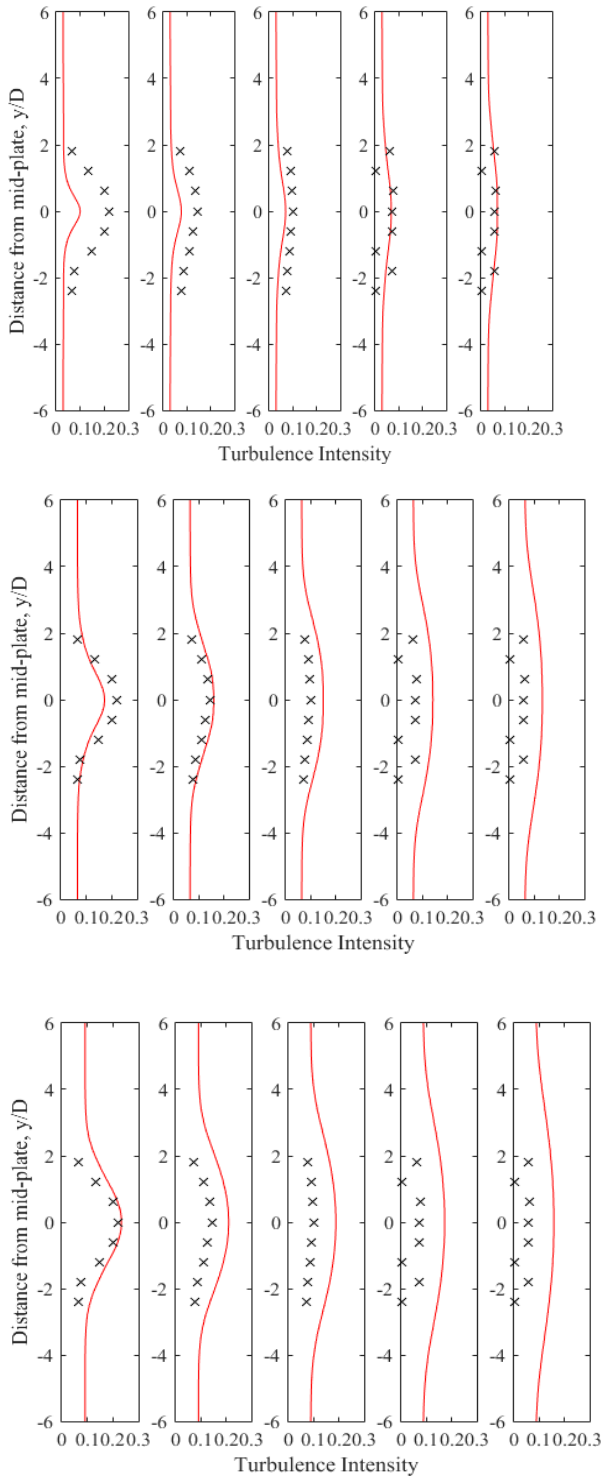

(b) Turbulence intensity at inlet turbulence intensity of 3% (Top) at 4D, 7D, 11D, 15D and 20D (shown from left to right), 7% (middle) at 4D, 7D, 11D, 15D and 20D (shown from left to right) and 10% (bottom) at 4D, 7D, 11D, 15D and 20D (shown from left to right).

Appendix 1: Velocity and turbulence intensity profiles of inlet turbulence intensities of 3% and 7% at 4D, 7D, 11D, 15D and 20D downstream of the disc. Comparison between numerical investigation and experimental results [7].

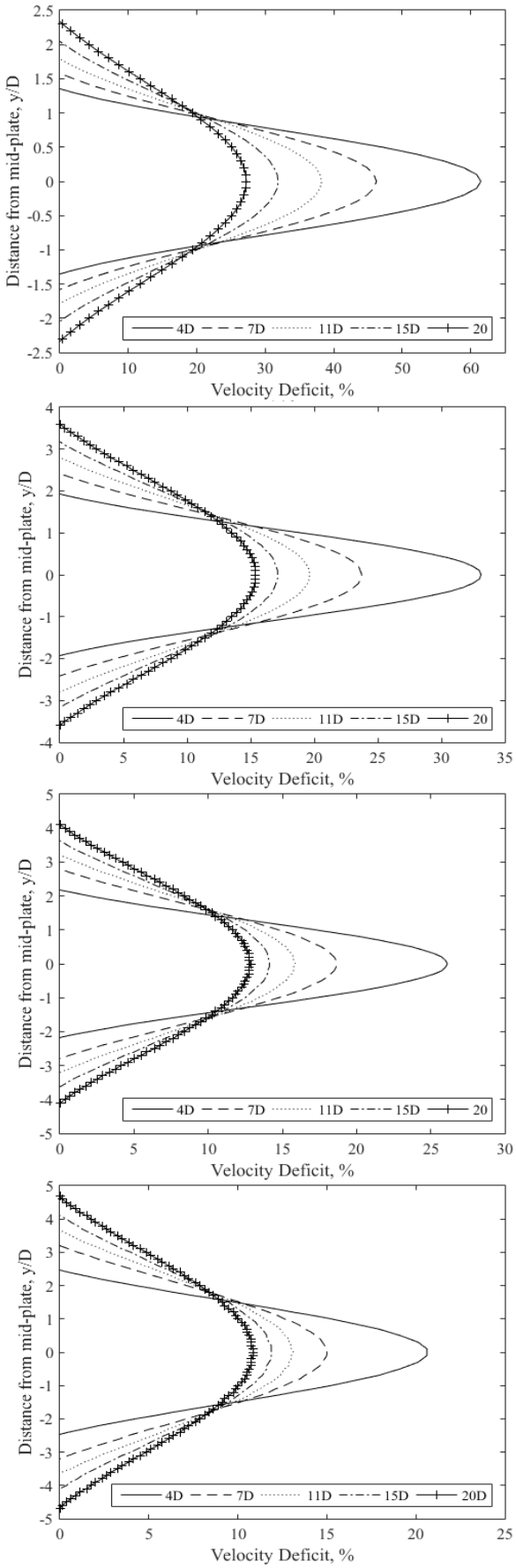

Appendix 2: Velocity wake profile of inlet turbulence intensities of 3%, 7%, 10% and 15% at 4D, 7D, 11D, 15D and 20D downstream of the disc.

REFERENCE

[1] F. O'Rourke, F. Boyle, and A. Reynolds, "Tidal current energy resource assessment in Ireland: Current status and future update," *Renew. Sustain. Energy Rev.*, vol. 14, no. 9, pp. 3206–3212, 2010.

[2] J. A. Clarke, G. Connor, A. D. Grant, and C. M. Johnstone, "Regulating the output characteristics of tidal current power stations to facilitate better base load matching over the lunar cycle," *Renew. Energy*, vol. 31, no. 2, pp. 173–180, 2006.

[3] F. O'Rourke, F. Boyle, and A. Reynolds, "Ireland's tidal energy resource; An assessment of a site in the Bulls Mouth and the Shannon Estuary using measured data," *Energy Convers. Manag.*, vol. 87, pp. 726–734, 2014.

[4] R. Vennell, "Exceeding the Betz limit with tidal turbines," *Renew. Energy*, vol. 55, pp. 277–285, 2013.

[5] Y. Chen, B. Lin, J. Lin, and S. Wang, "Experimental study of wake structure behind a horizontal axis tidal stream turbine," *Appl. Energy*, vol. 196, pp. 82–96, 2017.

[6] B. Morandi, F. Di Felice, M. Costanzo, G. P. Romano, D. Dhomé, and J. C. Allo, "Experimental investigation of the near wake of a horizontal axis tidal current turbine," *Int. J. Mar. Energy*, vol. 14, pp. 229–247, 2016.

[7] M. E. Harrison, W. M. J. Batten, L. E. Myers, and A. S. Bahaj, "A comparison between CFD simulations and experiments for predicting the far wake of horizontal axis tidal turbines," *Renew. Power Gener.*, vol. 4, no. 6, pp. 613–627, 2010.

[8] L. E. Myers and A. S. Bahaj, "Experimental analysis of the flow field around horizontal axis tidal turbines by use of scale mesh disc rotor simulators," *Ocean Eng.*, vol. 37, no. 2–3, pp. 218–227, 2010.

[9] N. Troldborg, J. N. Sørensen, and R. Mikkelsen, "Actuator line simulation of wake of wind turbine operating in turbulent inflow," *J. Phys. Conf. Ser.*, vol. 75, no. 1, 2007.

[10] R. Mikkelsen, *Actuator disc methods applied to wind turbines*. 2003.

[11] W. M. J. Batten, M. E. Harrison, and A. S. Bahaj, "The accuracy of the actuator disc-RANS approach for predicting the performance and far wake of a horizontal axis tidal stream turbine," *Philos. Trans. R. Soc. London A Math. Phys. Eng. Sci.*, vol. 371, no. 1985, 2013.

[12] V. T. Nguyen, S. S. Guillou, J. Thiébot, and A. Santa Cruz, "Modelling turbulence with an Actuator Disc representing a tidal turbine," *Renew. Energy*, vol. 97, pp. 625–635, 2016.

[13] P. Ouro, M. Harrold, L. Ramirez, and T. Stoesser, "Recent Advances in CFD for Wind and Tidal Offshore Turbines," no. February, 2019.

[14] ANSYS, *Ansys Release 5.6 Manual: Theory Reference*, Eleventh. Canonsburg, PA: ANSYS Inc., 1999.

[15] X. Sun, J. P. Chick, and I. G. Bryden, "Laboratory-scale simulation of energy extraction from tidal currents," *Renew. Energy*, vol. 33, no. 6, pp. 1267–1274, 2008.

[16] M. K. Das, P. P. Mukherjee, and K. Muralidhar, *Equations Governing Flow and Transport in Porous Media*. 2018.

[17] L. Myers and A. S. Bahaj, "Near wake properties of horizontal axis marine current turbines," *Proc. 8th Eur. Wave Tidal Energy Conf.*, pp. 558–565, 2009.

[18] V. Okulov, "The Lanchester–Betz–Joukowsky Limit," 2009.

[19] G. I. Taylor, *The Scientific Papers of Sir Geoffrey Ingram Taylor.* Cambridge University Press, 1963.

[20] J. Whelan, M. Thomson, J. M. R. Graham, and J. Peiro, "Modelling of free surface proximity and wave induced velocities around a horizontal axis tidal stream turbine," *Proc. 7th Eur. Wave Tidal Energy Conf. Porto Port.*, no. October, pp. 11–14, 2007.

[21] D. D. Apsley, T. Stallard, and P. K. Stansby, "Actuator-line CFD modelling of tidal-stream turbines in arrays," *J. Ocean Eng. Mar. Energy*, vol. 4, no. 4, pp. 259–271, 2018.

[22] B. Johnson, J. Francis, J. Howe, and J. Whitty, "Computational Actuator Disc Models for Wind and Tidal Applications," *J. Renew. Energy*, vol. 2014, pp. 1–10, 2014.